Structural Distortion of the Vanadyltetraphenylporphine Anion Radical Probed by Resonance Raman Spectroelectrochemistry

Ching-Yao Lin and Thomas G. Spiro*

Department of Chemistry, Princeton University, Princeton, New Jersey 08544

Received April 4, 1996[⊗]

Electronic effects of one-electron reduction are investigated for (OV)TPP (vanadyltetraphenylporphine) by the use of spectroelectrochemical techniques. Cyclic voltammetry (CV), absorption, and resonance Raman (RR) spectroscopy of the anion radical are analyzed with the aid of isotope labeling and normal-coordinate analysis (NCA) in order to understand the structural changes. The first reported Q-band excitation RR spectra of the (OV)TPP anion radical provide important information regarding the structural distortion of the porphyrin ring upon one-electron reduction, through detection of A_{2g} modes. Direct evidence for static distortion of the porphyrin ring is provided by the lowered depolarization ratios of the A_{2g} modes. Moreover, the upshift of the ν_{19} vibrational mode establishes that some of the C_α-C_m bonds are strengthened in the anion. Consideration of the molecular orbital pattern shows this observation to be consistent with a B_{1g} and not a B_{2g} Jahn−Teller distortion. The normal-mode calculation supports this inference.

Introduction

The π radicals of metalloporphyrins play important roles in many biological processes.[1] These anion and cation radical species are generated by one-electron oxidation or reduction of the porphyrin ring. There is growing interest in understanding their structure and dynamics.[2] Since the lowest unoccupied molecular orbital (LUMO, E_g*) is degenerate, anion radicals are subject to a structural distortion resulting from the Jahn−Teller effect. If the potential barrier between the two resulting states is larger than a vibrational quantum, a static distortion results and the symmetry is lowered from D_{4h} to D_{2h}. If the energy barrier is smaller than a vibrational quantum, the distortion is dynamic.

Because of its high sensitivity and selective enhancement for the vibrational modes of chromophores, resonance Raman (RR) spectroscopy is a useful probe of chromophore structure and has been increasingly applied to investigate the ground state,[3,4] excited state,[5−11] and π radical species[12−23] of many tetrapyrrolic chromophores. The nature of the J−T effect in radical anions can be characterized by examining depolarization ratios, enhancement patterns, and frequency shifts in RR spectra. In the case of metallo octaethylporphine (OEP) anion radicals, a static B_{1g} Jahn−Teller distortion has been established by resonance Raman (RR) spectroelectrochemical techniques.[24] The depolarization ratios observed in the RR spectra were found to deviate significantly from the values for a D_{4h} molecule, indicating symmetry lowering *via* a static Jahn−Teller distortion. In addition, many B_{1g} vibrational modes gained enhancement in the anion RR spectra, consistent with their becoming totally symmetric in the lowered molecular symmetry, D_{2h}. Moreover, vibrational frequency shifts of several structural marker bands were also consistent with a B_{1g} distortion.

Tetraphenylporphine (TPP) anions are less well characterized, although several RR spectra of the ZnTPP anion radical have been published.[12−15] Analysis has been hampered by band overlaps and by lack of structural marker bands, especially those deriving from non-totally symmetric modes, in Soret-excited RR spectra. Consequently, contradictory inferences have been drawn as to the nature of the structural changes.[13,14,25]

To remedy this situation, we have investigated vanadyltetraphenylporphine, (OV)TPP (Figure 1), using spectroelectro-

* To whom correspondence should be addressed.

⊗ Abstract published in *Advance ACS Abstracts,* August 15, 1996.

(1) Frew, J. E.; Jones, P. *Adv. Inorg. Bioinorg. Mech.* **1984**, *3*, 175.
(2) Fajer, J.; Davis, M. S. In *The Porphyrins*; Dolphin, D., Ed.; Academic Press: New York, 1978; Vol. 4, pp 197−256.
(3) Spiro, T. G., Ed. *Biological Applications of Raman Spectroscopy*; Wiley: New York, 1988; Vol. III.
(4) Ferraro, J. R.; Nakamoto, K. *Introductory Raman Spectroscopy*; Academic Press: New York, 1994; Chapter 4.
(5) Kumble, R.; Loppnow, G. R.; Hu, S.; Mukherjee, A.; Thompson, M. A.; Spiro, T. G. *J. Phys. Chem.* **1995**, *99*, 5809.
(6) Vitols, S. E.; Terashita, S.; Blackwood, M. E., Jr.; Kumble, R.; Ozaki, Y.; Spiro, T. G. *J. Phys. Chem.* **1995**, *99*, 7246.
(7) Bell, S. E. J.; Al-Obaidi, A. H. R.; Hegarty, M. J. N.; McGarvey, J. J.; Hester, R. E. *J. Phys. Chem.* **1995**, *99*, 3959.
(8) Sato, S.; Asano-Someda, M.; Kitagawa, T. *Chem. Phys. Lett.* **1992**, *1989*, 443.
(9) Bell, S. E. J.; Al-Obaidi, A. H. R.; Hegarty, M. J. N.; Hester, R. E.; McGarvey, J. J. *J. Phys. Chem.* **1993**, *97*, 11599.
(10) Kumble, R.; Hu, S.; Loppnow, G. R.; Vitols, S. E.; Spiro, T. G. *J. Phys. Chem.* **1993**, *97*, 10521.
(11) Waters, V. A.; de Paula, J. C.; Babcock, G. T.; Leroi, G. E. *J. Am. Chem. Soc.* **1989**, *111*, 8300.
(12) Anxolabéhère, É.; Chottard, G.; Lexa, D. *New. J. Chem.* **1994**, *18*, 889.
(13) Reed, R. A.; Purrello, R.; Prendergast, K.; Spiro, T. G. *J. Phys. Chem.* **1991**, *95*, 9720.
(14) Atamian, M.; Donohoe, R. J.; Lindsey, J. S.; Bocian, D. F. *J. Phys. Chem.* **1989**, *93*, 2236.
(15) Yamaguchi, H.; Soeta, A.; Toeda, H.; Itoh, K. *J. Electroanal. Chem. Interfacial Electrochem.* **1983**, *159*, 347.
(16) Kim, D.; Miller, L. A.; Rakhit, G.; Spiro, T. G. *J. Phys. Chem.* **1986**, *90*, 3320.
(17) Czernuszewicz, R. S.; Macor, K. A.; Li, X.-Y.; Kincaid, J. R.; Spiro, T. G. *J. Am. Chem. Soc.* **1989**, *111*, 3860.
(18) Macor, K. A.; Czernuszewicz, R. S.; Spiro, T. G. *Inorg. Chem.* **1990**, *29*, 1996.
(19) Salehi, A.; Oertling, W. A.; Babcock, G. T.; Chang, C. K. *J. Am. Chem. Soc.* **1986**, *108*, 5630.
(20) Oertling, W. A.; Salehi, A.; Chang, C. K.; Babcock, G. T. *J. Phys. Chem.* **1987**, *91*, 3114.
(21) Oertling, W. A.; Salehi, A.; Chung, Y. C.; Leroi, G. E.; Chang, C. K.; Babcock, G. T. *J. Phys. Chem.* **1987**, *91*, 5887.
(22) Oertling, W. A.; Salehi, A.; Chang, C. K.; Babcock, G. T. *J. Phys. Chem.* **1989**, *93*, 1311.
(23) Hashimoto, S.; Mizutani, Y.; Tatsuno, Y.; Kitagawa, T. *J. Am. Chem. Soc.* **1991**, *13*, 6542.
(24) Hu, S.; Lin, C.-Y.; Blackwood, M. E., Jr.; Mukherjee, A.; Spiro, T. G. *J. Phys. Chem.* **1995**, *99*, 9694.
(25) Seth, J.; Bocian, D. F. *J. Am. Chem. Soc.* **1994**, *116*, 143.

S0020-1669(96)00381-3 CCC: $12.00

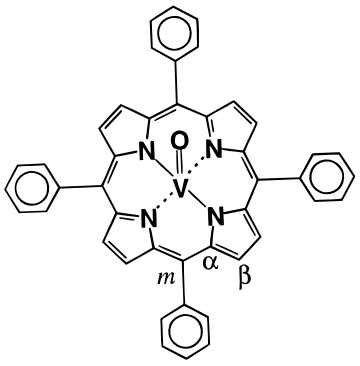

Figure 1. Molecular structure and labeling scheme for vanadyltetraphenylporphine.

chemical techniques. (OV)TPP was chosen because the electron-withdrawing vanadyl (V═O) group leads to formation of a more stable anion radical at less negative potential and eliminates the possibility of generating phlorin, which can interfere with the characterization of porphyrin anion radicals.[15,26] As a result, we are able to report the first Q-band excitation RR spectra of a metalloporphyrin anion radical. These spectra reveal depolarization ratio changes and frequency shifts of A_{2g} vibrational bands, which provide critical information on the nature of the Jahn−Teller distortion.

Experimental Section

Materials. H_2TPP and its $^{15}N_4$, *meso*-$^{13}C_4$, [β-D_8]pyrrole, and [D_{20}]-phenyl isotopomers were prepared according to the method of Lindsey *et al*.[27] Introduction of the vanadyl ion into H_2TPP was carried out in a 1:2 pyridine/acetic acid mixed solution reflux for 4 h, using a 100-fold excess of vanadyl sulfate. The completeness of the metalation was monitored with a UV−vis spectrometer. An equal volume of deionized water was added to the cooled solution after the reflux was completed, followed by suction filtration to collect the precipitated (OV)TPP. The product was further purified by column chromatography (silica gel/CH_2Cl_2) and recrystallization to remove trace amounts of impurities and of unreacted H_2TPP.

Anhydrous tetrahydrofuran (THF) was distilled in the presence of sodium and benzophenone under argon and degassed by at least three freeze−pump−thaw cycles before being used in a glovebox for the spectroelectrochemistry experiments.

Electrochemistry and Spectroelectrochemistry. Cyclic voltammetry (CV) was performed with the use of a Bioanalytical Systems Model BAS CV-27 potentiostat and a three-electrode cell. A glassy carbon electrode (GCE) was used as the working electrode. A platinum wire, used as the auxiliary electrode, was isolated from the main compartment by a fine glass frit. A saturated calomel electrode (SCE) was used as the reference electrode and was also isolated from the main compartment by a junction with a platinum wire on the tip. For controlled-potential electrolysis, a Princeton Applied Research Model 173 potentiostat was used to control the potential.

UV−vis spectroelectrochemistry was performed with an airtight, optically transparent thin-layer electrochemical (OTTLE) cell constructed with a 100 mesh platinum gauze working electrode in a 1 mm quartz cell. Reference and counter electrodes were separately isolated from the main compartment by a fine glass frit. Spectra were obtained with a Hewlett Packard diode array 8451A UV−vis spectrophotometer. The bulk electrolysis cell for resonance Raman experiments has been described previously.[28] Both OTTLE and electrolysis cells were assembled under an inert atmosphere in a glovebox equipped with a Dri-train to exclude moisture and oxygen. The absence of phlorin after bulk electrolysis was checked spectrophotometrically.

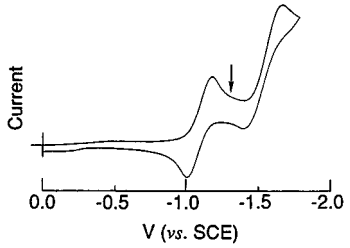

Figure 2. Cyclic voltammogram of (OV)TPP in THF/0.1 M TBAP. The arrow indicates the applied potential used to carry out controlled-potential electrolysis.

Resonance Raman spectra were obtained in backscattering geometry from THF solution in a bulk electrolysis RR cell. Excitation lines were provided with a Coherent Innova 100K3 krypton ion laser (568.2 and 647.1 nm) and with a Liconix helium−cadmium laser (441.7 nm). The scattered light was collected and dispersed with a Spex 1404 double monochromator equipped with a cooled photomultiplier (RCA 31034A-02).

Normal-Mode Calculation. The **GF** matrix method of Wilson was used to carry out a normal-mode calculation for the anion radicals of vanadyltetraphenylporphine, commencing with the valence force field developed for NiTPP.[29a] The symmetry coordinates ($\mathbf{S}_i$) and the corresponding **U** matrix were obtained from a symmetry-adapted linear combination of bond stretching and angle bending internal coordinates. A menu-driven, graphically-interfaced version[30] of Schachtschneider's programs was used to set up the **G** matrix and to solve the secular equation, $|\mathbf{GF} - \mathbf{E}\lambda| = 0$. The vanadyl (O═V) group was treated as a point mass in the calculation because the in-plane porphyrin modes are not expected to couple significantly with the V−O motions. A D_{4h} model was used to calculate vibrations for the neutral (OV)TPP, and a D_{2h} molecule was used to carry out the calculation for the anion radical. The structural parameters used in the calculation are the same as those of NiTPP[29a] and are nearly identical to those of (OV)TPP.[29c]

Results

Electrochemistry and UV−Vis Spectroscopy. Figure 2 shows the cyclic voltammogram (CV) of (OV)TPP in THF/0.1 M TBAP solution. Two well-separated reduction reactions were observed at −1.10 and −1.55 V (*vs* SCE). The first redox couple is quasi-reversible and is believed to be the reduction of (OV)TPP to its anion radical while the second one is the reduction to the dianion species.[31,32] Both the first and second reduction potentials are similar to the reported values[31,32] and are less negative than those of ZnTPP (−1.31 and −1.72 V *vs* SCE for the first and second reductions, respectively)[15,26, 33−36] because the vanadyl group is more electron-withdrawing than Zn^{2+}. The arrow in the figure indicates the applied potential used to carry out the spectroelectrochemical studies.

(26) Closs, G. L.; Closs, L. E. *J. Am. Chem. Soc*. **1963**, *85*, 818.
(27) (a) Lindsey, J. S.; Hsu, H. C.; Schreiman, I. C. *Tetrahedron Lett*. **1986**, *27*, 4969. (b) Lindsey, J. S.; Schreiman, I. C.; Kearney, P. C.; Marguerettaz, A. M. *J. Org. Chem*. **1987**, *52*, 827.
(28) Czernuszewicz, R. S.; Macor, K. A. *J. Raman Spectrosc*. **1988**, *19*, 553.
(29) (a) Li, X.-Y.; Czernuszewicz, R. S.; Kincaid, J. R.; Su, Y. O.; Spiro, T. G. *J. Phys. Chem*. **1990**, *94*, 31. (b). Li, X.-Y.; Czernuszewicz, R. S.; Kincaid, J. R.; Stein, P.; Spiro, T. G. *J. Phys. Chem*. **1990**, *94*, 47. (c) Drew, M. G. B.; Mitchell, P. C. H.; Scott, C. E. *Inorg. Chim. Acta* **1984**, *82*, 63.
(30) Mukherjee, A.; Spiro, T. G. *QCPE Bull*. **1995**, *15* (1), Program 656.
(31) Kadish, K. M.; Sazou, D.; Araullo, C.; Liu, Y. M.; Saoiabi, A.; Ferhat, M.; Guilard, R. *Inorg. Chem*. **1988**, *27*, 2313.
(32) Kadish, K. M.; Morrison, M. M. *Bioinorg. Chem*. **1977**, *7*, 107.
(33) Seely, G. R.; Gust, D.; Moore, T. A.; Moore, A. L. *J. Phys.Chem*. **1994**, *98*, 10659.
(34) Felton, R. H.; Linschitz, H. *J. Am. Chem. Soc*. **1966**, *88*, 1113.
(35) Kadish, K. M.; Shiue, L. R.; Rhodes, R. K.; Bottomley, L. A. *Inorg. Chem*. **1981**, *20*, 1274.
(36) Clack, D. W.; Hush, N. S. *J. Am. Chem. Soc*. **1965**, *87*, 4238.
(37) Prendergast, K.; Spiro, T. G. *J. Am. Chem. Soc*. **1992**, *114*, 3793.
(38) Sekino, H.; Kobayashi, H. *J. Chem. Phys*. **1987**, *86*, 5045.
(39) Lin, M.; Lee, M.; Yue, K. T.; Marzilli, L. G. *Inorg. Chem*. **1993**, *32*, 3217.
(40) Su, Y. O.; Czernuszewicz, R. S.; Miller, L. A.; Spiro, T. G. *J. Am. Chem. Soc*. **1988**, *110*, 4150.

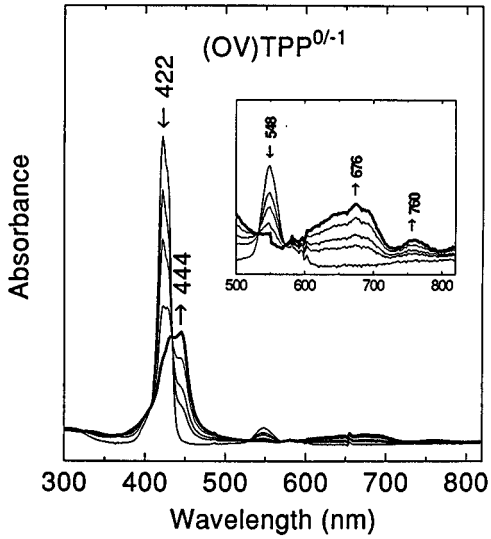

Figure 3. UV−vis spectral changes of (OV)TPP during the thin-layer electrolysis in THF. The bold line represents the trace for the (OV)-TPP anion radical. Applied potential: −1.30 V vs SCE.

Figure 3 shows the UV−vis spectral changes during the electrolysis of (OV)TPP to its anion radical. The bold line represents the trace for the (OV)TPP anion radical. Isosbestic points found at 324, 406, 434, 528, and 572 nm indicate that no detectable intermediate was formed during the conversion of (OV)TPP to the anion radical. The Soret band red-shifted from 422 to 444 nm while the two Q-bands moved from 548 and 592 nm to 676 and 760 nm; the $(OV)TPP^-$ band maxima are close to the reported values for the ZnTPP anion radical.[15,26] There was no evidence for the formation of phlorin[26] during the electrolysis, and more than 98% of the neutral (OV)TPP was recovered when the anion radical was reoxidized to the neutral species (spectrum not shown).

Resonance Raman Spectroelectrochemistry. Figures 4 and 5 compare the RR spectra of (OV)TPP and the anion radical with 441.7 nm (Soret) excitation in the high- and low-frequency regions, respectively. Soret-excited RR spectra of NA (natural abundance), $^{13}C_4$, and D_8 $(OV)TPP^-$ are collected in Figure 6. Spectra are not shown for the neutral parent of each isotopomer because the intensity patterns and isotope shifts are nearly identical to those observed for NiTPP.[29a] Figure 7 compares the Q-band excitation RR spectra of NA-(OV)TPP (568.2 nm) with its anion radical (647.1 nm) and D_8-(OV)TPP anion radical. In these figures, both the parallel and the perpendicular traces of the spectra for each species are shown, while the vibrational frequencies and the depolarization ratios of selected modes are listed in Table 1 for (OV)TPP and its anion radical. Mode assignments and the correlation between the neutral species and the anion radical were made on the basis of the reported vibrational frequencies of (OV)TPP in CH_2Cl_2,[18] correspondences with NiTPP vibrational frequencies,[29a] depolarization ratios, and isotope shifts. Several vibrational modes (ν_2, ν_4, ν_6, ν_{10}, ν_{11}, ν_{17}, ν_{19}, ν_{20}, and ν_{26}) were shifted upon porphyrin ring reduction (Table 1), as noted before for ZnTPP.[12−15] Additionally, the depolarization ratios of the (OV)TPP anion radical were found to be different from those of the neutral parent. The depolarization ratios of D_{4h}−A_{1g} modes increase, while those of B_{1g} and A_{2g} modes decrease. This phenomenon is especially significant for ν_{19}, ν_{20}, and ν_{26} (A_{2g}) modes, whose depolarization ratios are infinity for (OV)TPP but less than 2.1 for $(OV)TPP^-$. The altered depolarization ratios indicate that symmetry of the molecule is lowered upon one-electron reduction.

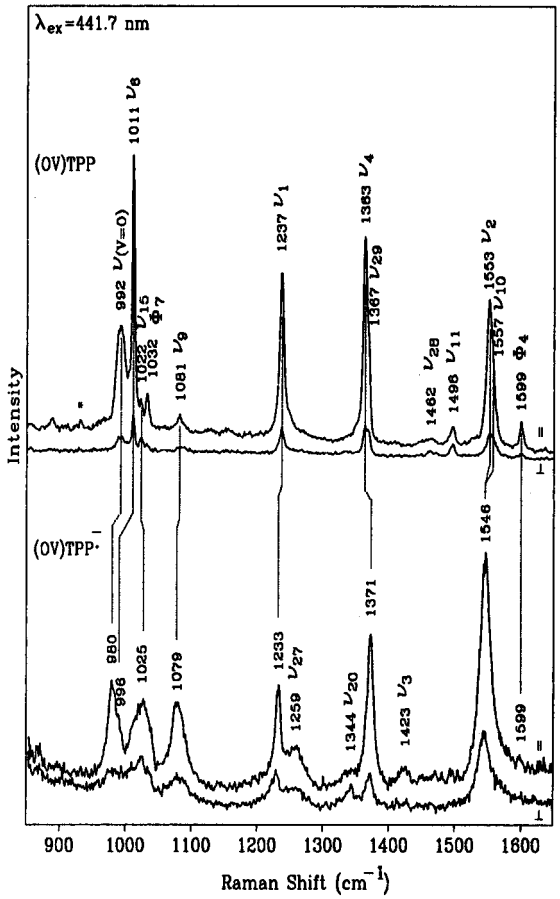

Figure 4. RR spectra of (OV)TPP and its anion radical obtained with excitation at 441.7 nm in THF (solvent signals subtracted). The asterisk indicates the 934 cm^{-1} ν_1 band of ClO_4^- (electrolyte). Conditions: 4 cm^{-1} slit width, one scan for the neutral (OV)TPP and two scans coadded for the anion radical with 1 cm^{-1}/s increment, applied potential −1.30 V vs SCE.

Table 1. Comparison of Observed RR Frequencies (cm^{-1}) and Depolarization Ratios of (OV)TPP and the Anion Radical

		frequency (ρ)	
symmetry	mode	(OV)TPP	(OV)TPP anion radical
A_{1g}	ν_2	1554 (0.15)	1546 (0.35)[a]
	ν_4	1363 (0.14)	1371 (0.23)
	ν_1	1237 (0.15)	1233 (0.28)
	ν_9	1081 (0.18)	1079 (0.36)
	ν_6	1010 (0.14)	996 (0.43)
	ν_8	397 (0.13)	396 (0.24)
B_{1g}	ν_{10}	1557 (0.25)[b]	1546 (0.35)[a]
	ν_{11}	1496 (0.72)	1467
	ν_{17}	1082 (0.67)	1071 (0.38)
A_{2g}	ν_{19}	1513 (∞)	1540 (2.02)[c]
	ν_{20}	1335 (∞)	1344 (1.67)
	ν_{26}	1241 (∞)	1225 (1.38)

[a] ν_2 and ν_{10} are overlapped in the anion RR spectrum. [b] Depolarization ratio of ν_{10} is uncertain due to overlapping with ν_2 in (OV)TPP RR spectrum. [c] Measured from the D_8-(OV)TPP anion RR spectrum.

This is the first study to report a porphyrin radical RR spectrum with excitation in the Q-band. Absorption in the visible region is weak and broad (Figure 3), and RR scattering is correspondingly weak. Nevertheless, we were able to obtain a good-quality RR spectrum with 647.1 nm excitation (Figure 7). Q-band excitation produces very different RR enhancement patterns for neutral metalloporphyrins,[29a,b] and these differences are also detectable for $(OV)TPP^-$: non-totally symmetric modes (ν_{19}, ν_{20}, ν_{26}, ν_{17}, ν_{15}, *etc.*) gain significant intensity, although

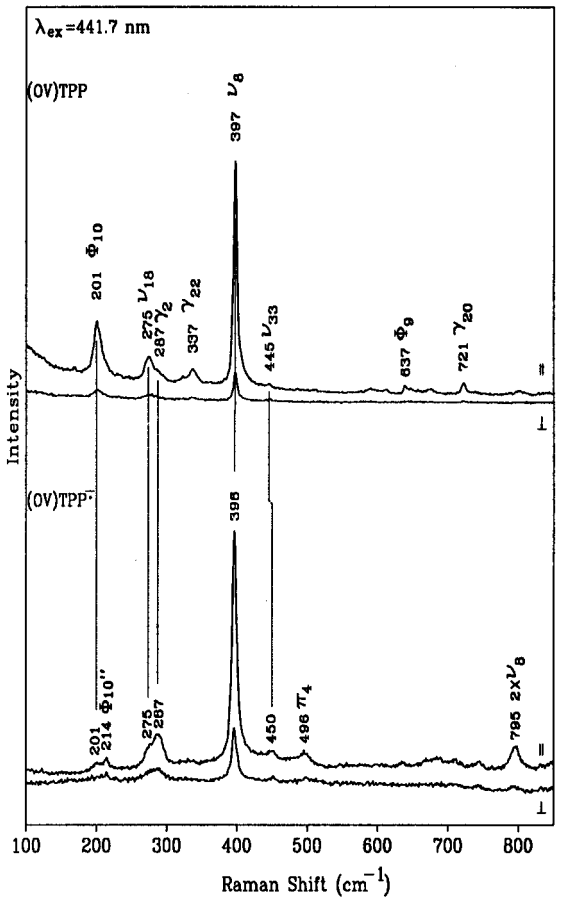

Figure 5. As Figure 4, but in the low-frequency region.

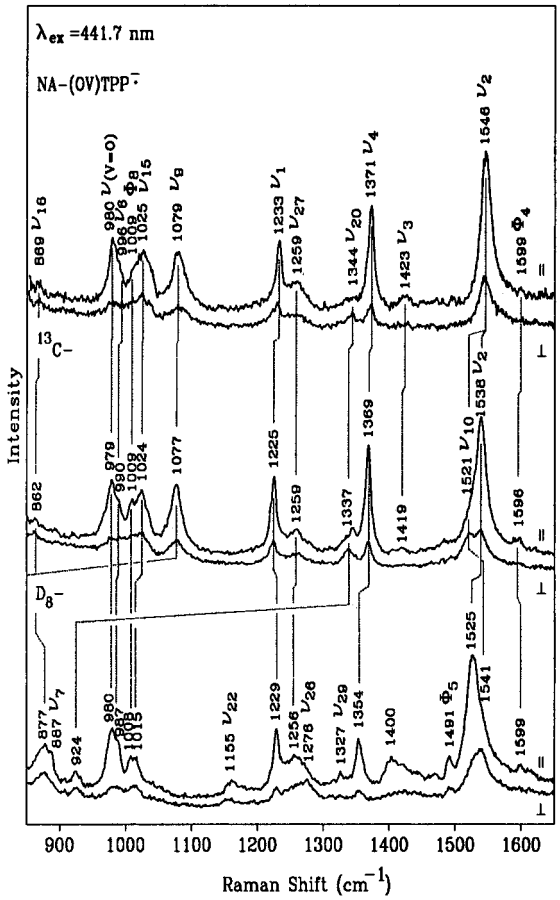

Figure 6. 441.7 nm excited RR spectra of the (OV)TPP anion radical and the indicated isotopomers.

ν_4 and ν_2 are still strong in the Q-band excitation RR spectra. ν_{19} and ν_2 are overlapped for the NA-(OV)TPP anion radical (Figure 7); these two modes were resolved with the aid of deuteration at the pyrrole β positions (D_8-OVTPP$^-$ spectrum). Significantly, ν_{19} shifts up by 27 cm^{-1} upon one-electron reduction of (OV)TPP.

Non-totally symmetric modes are not strongly enhanced in the Soret-excited RR spectrum of (OV)TPP$^-$ (Figure 4). Two of them (ν_{15} and ν_{27}), however, are stronger than in the neutral parent. For (OV)OEP$^-$, several B_{1g} and B_{2g} modes became strongly enhanced as the excitation wavelength was shifted through the complex Soret absorption band.[24] Changing excitation wavelength did not affect the (OV)TPP$^-$ RR intensity pattern, however.

Most of the anion radical RR bands are reliably assigned with the aid of the depolarization ratios and isotope shifts. However, D_8-(OV)TPP$^-$ RR spectra (Figures 6 and 7) contain complex bands at ~1400 cm^{-1} which result from overlap of ν_3, ν_{11}, and ν_{28} modes.

Normal-Coordinate Analysis. In order to understand the structural changes of (OV)TPP upon one-electron reduction, we carried out a normal-coordinate analysis. Initial parameters were taken from the force field developed for NiTPP.[29a] Calculated and observed frequencies are compared in Tables 2 and 3 for neutral (OV)TPP and the anion radical, respectively. The final force fields are tabulated in Table 4. The eigenvector plots of four selected (OV)TPP anion radical vibrational modes are diagrammed in Figure 8. The oxygen atom of the V=O group was omitted in the calculation, since the V−O motions are not expected to couple significantly with the in-plane porphyrin vibrations. The experimental depolarization ratios of neutral (OV)TPP (Table 1) are very close to the theoretical values[41] for a D_{4h} molecule (1/8, infinity, 3/4, and 3/4 for A_{1g}, A_{2g}, B_{1g}, and B_{2g} vibrational modes, respectively), justifying a D_{4h} model for the calculation. The NiTPP force constants were altered to improve the fit to (OV)TPP frequencies: (1) the stretching force constants were lowered in accord with the altered core size;[37] (2) the C−C_β−H bending force constants and their interactions were changed slightly to reflect the smaller separation between ν_9 and ν_{17} in (OV)TPP than in NiTPP; (3) several 1,2 and 1,3 stretch−stretch interactions were also changed to adjust the spacing of ν_2, ν_{10}, and ν_{19}, *i.e.* to increase the frequency of ν_{19} while slightly lowering the frequencies of ν_2 and ν_{10}.

For the (OV)TPP anion radical, the symmetry of the molecule in the calculation was reduced to D_{2h} because we found it is impossible to reproduce the disparate frequency shift patterns of two C_β−C_β stretching modes, ν_2 (7 cm^{-1}) and ν_{11} (29 cm^{-1}), by using a D_{4h} model, as previously noted for (OV)OEP$^-$.[24] This is expected because these two modes largely consist of C_β−C_β bond stretching for (OV)TPP$^-$ (Table 3), differing only in their phasing (Figure 8). Varying the C_β−C_β stretching force constant, $K(C_\beta{-}C_\beta)$, in a D_{4h} calculation shifts these two modes in the same direction by similar magnitudes. The frequency shift pattern was modeled by relaxing the symmetry constraints on the force field from D_{4h} to D_{2h}, in which $K(C_\beta{-}C_\beta)$ splits into two sets of force constants. The final force constants of (OV)TPP and its anion radical are listed in Table 4, along with those of NiTPP. The required force constant changes not only reproduce the disparate frequency shifts of the two C_β−C_β

(41) (a) Clark, R. J. H.; Dines, T. J. *Angew. Chem., Int. Ed. Engl.* **1986**, *25*, 131. (b) Spiro, T. G.; Strekas, T. C. *Proc. Natl. Acad. Sci. U.S.A.* **1972**, *69*, 2622.
(42) Burgi, H.; Dunitz, J. D. *J. Am. Chem. Soc.* **1987**, *109*, 2924.

Table 2. Comparison of Observed and Calculated Frequencies (cm^{-1}) of Selected (OV)TPP Vibrations[a]

		obsd					calcd				
		NA	$\Delta(^{15}N_4)$	$\Delta(^{13}C_4)$	$\Delta(D_8)$	$\Delta(D_{20})$	NA	$\Delta(^{15}N_4)$	$\Delta(^{13}C_4)$	$\Delta(D_8)$	$\Delta(D_{20})$
A_{1g}	ν_2	1553	0	8	21	4	1550	0	9	9	10
	ν_3				(1433)		1444	0	10	29	−13
	ν_4	1363	7	1	9	3	1365	6	5	16	25
	ν_1	1237	2	8	1	50	1227	7	3	6	31
	ν_9	1081	2	0	306	−3	1083	0	1	311	10
	ν_6	1010	18	1	4	5	1012	11	1	−2	6
	ν_8	397	2	0	8	1	398	3	0	8	1
B_{1g}	ν_{10}	1557	0	21	4		1562	1	29	2	0
	ν_{11}	1496	1	1	48	1	1495	1	1	47	0
	ν_{17}	1082					1076	0	0	307	0
	ν_{15}	1022	9	3		1	1018	7	4	10	0
A_{2g}	ν_{19}	1513			3		1512	0	31	1	0
	ν_{20}	1335	0	9	482		1341	0	0	495	0
	ν_{26}	1241			−30	0	1241	7	4	−20	0
B_{2g}	ν_{28}	1462	2	5		−6	1459	0	14	5	−24
	ν_{29}	1367	0	7	38	14	1366	0	5	50	21

[a] Negative isotope shifts indicate upshifts of modes upon isotope labeling.

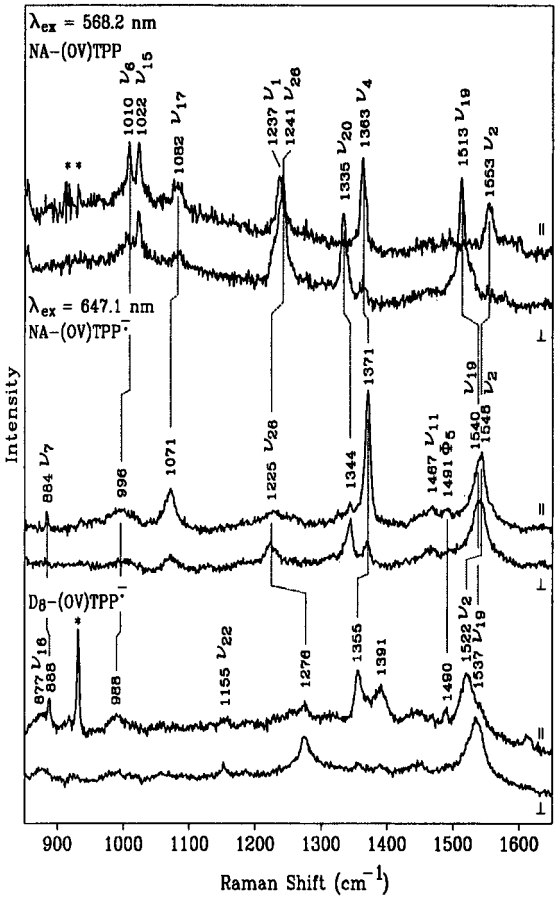

Figure 7. Q-Band-excited RR spectra of (OV)TPP (568.2 nm) and the anion radicals (647.1 nm), including the D_8 isotopomer (conditions as in Figure 4, except that two scans were coadded for the neutral species and five scans for the anion radicals).

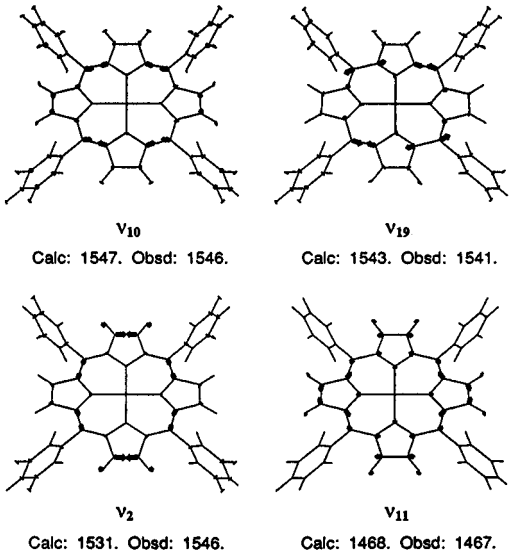

Figure 8. Eigenvector plots for selected vibrations of the (OV)TPP anion radical.

stretching modes, but alter the normal-mode compositions as well. As illustrated in Figure 8, ν_2 and ν_{11} vibrations are now much more localized than those of the neutral parent. This localization phenomenon results from the inequivalent $C_\beta-C_\beta$ bonds for the anion radical.

The $C_\alpha-C_m$ stretching modes, ν_{10} and ν_{19} (Figure 8), shift in opposite directions upon one-electron reduction (27 cm^{-1} upshift for ν_{19}; 11 cm^{-1} downshift for ν_{10}). Reproducing this effect required introduction of 1,4 and 1,5 ($C_\alpha-C_m$) bond interactions in the normal-mode calculation. Other force constants were slightly altered to better fit the $(OV)TPP^-$ frequencies.

Discussion

Decreased Depolarization Ratios of A_{2g} Vibrations: Direct Evidence for Static Distortion. The symmetry lowering of metalloporphyrins can be detected by measuring the depolarization ratio of Raman bands, ρ, the intensity ratio for scattering perpendicular and parallel to the incident polarization. For D_{4h} metalloporphyrins, $\rho = 1/8$, 3/4, 3/4, and ∞ for Raman-active vibrational modes with A_{1g}, B_{1g}, B_{2g}, and A_{2g} symmetries, respectively.[41] When the symmetry of a metalloporphyrin is lowered from D_{4h} to D_{2h}, A_{1g} and B_{1g} modes become totally symmetric (A_g), while A_{2g} and B_{2g} modes transform as B_{1g}. Therefore, modes correlating with A_{1g} and B_{1g} have depolarization ratios between 1/8 and 3/4, while those correlating with A_{2g} and B_{2g} have depolarization ratios between 3/4 and infinity. This situation is encountered, for example, in metallobacteriochlorins, in which two opposite pyrrole rings are reduced.[43]

The depolarization ratios of neutral (OV)TPP (Table 1) are close to the theoretical values for a D_{4h} molecule. In contrast,

Table 3. Observed and Calculated Frequencies (cm^{-1}) for the (OV)TPP Anion Radical and Its Isotopomers[a]

		obsd					calcd					
		NA	$\Delta(^{15}N)$	$\Delta(^{13}C)$	$\Delta(D_8)$	$\Delta(D_{20})$	NA	$\Delta(^{15}N)$	$\Delta(^{13}C)$	$\Delta(D_8)$	$\Delta(D_{20})$	assignment (PED, %)
A_g	ν_{10}	1546	1	25	5	3	1547	0	16	4	8	46% $\nu(C_\alpha C_m)$, 17% $\nu(C_pC_p)$
	ν_2	1546	1	8	21	3	1531	0	8	24	2	49% $\nu(C_\beta C_\beta)$, 20% $\nu(C_\alpha C_m)$*, 8% $\delta(C_\alpha C_\beta H)$
	ν_{11}	1467					1468	2	8	26	0	25% $\nu(C_\alpha C_m)$*, 18% $\nu(C_\beta C_\beta)$, 17% $\nu(C_\beta C_\beta)$*, 17% $\nu(C_\alpha C_\beta)$*, 15% $\nu(C_\alpha C_m)$
	ν_3	1423		4			1424	0	10	22	−14	42% $\nu(C_\beta C_\beta)$*, 18% $\nu(C_\alpha C_m)$*, 7% $\nu(C_1C_m)$
	ν_4	1371	7	2	17	12	1373	5	8	27	31	20% $\nu(C_\alpha C_\beta)$*, 11% $\nu(C_\alpha C_\beta)$, 11% $\nu(C_\alpha N)$*, 10% $\delta(C_\alpha C m C_\alpha)$
	ν_1	1233	4	8	4	51	1221	8	2	9	29	20% $\nu(C_\alpha N)$, 18% $\nu(C_1C_m)$, 12% $\nu(C_\alpha N)$*, 15% $\delta(C_pC_pH)$
	ν_9	1079	4	2	306	3	1085	0	0	306	3	32% $\delta(C_\beta C_\beta H)$, 24% $\delta(C_\alpha C_\beta H)$, 6% $\nu(C_\beta C_\beta)$
	ν_{17}	1071					1078	4	2	322	8	24% $\nu(C_\alpha C_\beta)$*, 13% $\delta(C_\beta C_\beta H)$*, 10% $\delta(C_\alpha C_\beta H)$*
	ν_{15}	1025	7	1	10	1	1029	8	2	−10	0	20% $\delta(C_\beta C_\beta H)$*, 18% $\delta(C_\alpha C_\beta H)$*, 15% $\nu(C_\alpha C_\beta)$*, 15% $\nu(C_\alpha N)$*
	ν_6	996	5	6	9		1005	18	2	2	5	31% $\nu(C_\alpha C_\beta)$, 11% $\nu(C_\alpha N)$, 9% $\delta(C_pC_pC_p)$, 6% $\delta(C_1C_pC_p)$
	ν_8	396	2	0	8	0	397	3	0	8	0	16% $\delta(C_\alpha C_m C_\alpha)$, 13% ν(NV)*, 12% ν(NV), 6% $\nu(C_\alpha C_m)$*
B_{1g}	ν_{19}	1540			3		1543	0	28	2	4	64% $\nu(C_\alpha C_m)$, 16% $\nu(C_\alpha C_m)$*, 6% $\nu(C_pC_p)$
	ν_{20}	1344	2	7	420		1348	0	2	523	10	36% $\delta(C_\beta C_\beta H)$, 30% $\nu(C_\alpha C_\beta)$, 19% $\delta(C_\alpha C_\beta H)$, 7% $\delta(C_\alpha C_\beta C_\beta)$
	ν_{27}	1259	7	1	3	1	1269	8	3	−5	21	38% $\nu(C_\alpha N)$*, 15% $\nu(C_1C_m)$, 9% $\delta(C_\beta C_\alpha N)$*, 8% $\delta(C_\alpha C_\beta C_\beta)$*
	ν_{26}	1225			−51	2	1228	8	5	−10	3	39% $\nu(C_\alpha N)$, 11% $\nu(C_\alpha N)$*, 9% $\delta(C_\alpha C_\beta H)$*, 9% $\delta(C_\alpha C_\beta C_\beta)$

[a] Asterisks indicate chemical bonds in or adjacent to the pyrroles with weakened $C_\beta-C_\beta$ bonds. Negative shifts represent upshifts of vibrations upon isotope labeling. PED: potential energy distribution.

Table 4. Force Constants Used for NiTPP, (OV)TPP and (OV)TPP Anion Radical Normal-Mode Calculations[a]

force const	NiTPP	(OV)TPP
$\nu(C_\alpha C_m)$	6.98	6.60
$\nu(C_\alpha C_\beta)$	5.02	5.02
$\nu(C_\beta C_\beta)$	7.12	7.11
$\nu(C_\alpha N)$	5.64	5.20
1,2-$(C_\alpha C_m)(C_\alpha C_m)$	0.60	0.59
1,3-$(C_\alpha C_m)(C_\beta C_\beta)$	−0.30	−0.15
1,3-$(C_\alpha C_m)(C_\alpha C_\beta)$	−0.15	−0.25
1,3-$(C_\alpha C_m)(C_\alpha N)$	−0.15	−0.05
$\delta(C_\beta C_\beta H)$	0.454	0.434
$\delta(C_\alpha C_\beta H)$	0.454	0.434
1,2-$(C_\alpha C_\beta)(C_\alpha C_\beta H)$	0.00	0.10
1,2-$(C_\beta C_\beta)(C_\beta C_\beta H)$	0.10	0.15

force const	(OV)TPP (D_{4h})	(OV)TPP$^-$ (D_{2h})
$\nu(C_\alpha C_m)$	6.60	6.80
$\nu(C_\alpha C_m)$*		5.85
$\nu(C_\alpha C_\beta)$	5.02	4.82
$\nu(C_\alpha C_\beta)$*		5.72
$\nu(C_\beta C_\beta)$	7.11	7.31
$\nu(C_\beta C_\beta)$*		6.61
$\nu(C_\alpha N)$	5.20	5.00
$\nu(C_\alpha N)$*		5.20
1,4-$(C_\alpha C_m)(C_\alpha C_m)$	0.0	−0.15
1,4-$(C_\alpha C_m)$*$(C_\alpha C_m)$*		0.00
1,5-$(C_\alpha C_m)(C_\alpha C_m)$*	0.0	0.15
1,3-$(C_\alpha C_m)(C_\beta C_\beta)$	−0.15	−0.40
1,3-$(C_\alpha C_m)$*$(C_\beta C_\beta)$*		−0.15
$\delta(C_\beta C_\beta H)$	0.434	0.454
$\delta(C_\beta C_\beta H)$*		0.404

[a] For (OV)TPP$^-$, the number of force constants is doubled due to symmetry lowering to D_{2h} in the normal-mode calculation. Asterisks indicate chemical bonds in or adjacent to the pyrroles with weakened $C_\beta-C_\beta$ bonds for the anion radical. Force constant units: stretching, mdyn/Å; bending, mdyn Å/rad^2.

the depolarization ratios of the (OV)TPP anion radical deviate from D_{4h} values; the depolarization ratios of the formerly A_{1g} modes increase while those of the formerly B_{1g} modes decrease. However, the deviation is not as obvious as was found in (OV)OEP$^-$ RR spectra.[24] For (OV)OEP, polarized bands (ν_2, ν_3, ν_4, and ν_5) are well resolved from depolarized bands (ν_{10}, ν_{11}, ν_{29}, and ν_{13}) in the neutral parent RR spectra, and these modes did not overlap when the complex was reduced to the anion radical. However, in the case of (OV)TPP, polarized bands (ν_2, ν_4, and ν_6) overlap with depolarized bands (ν_{10}, ν_{29}, and ν_{15}) in Soret-excited RR spectra. Moreover, these bands remained overlapped for (OV)TPP$^-$ (Figure 4). This overlap phenomenon has made it difficult to interpret TPP anion spectra previously.[13]

The clearest evidence for symmetry lowering is provided by the A_{2g} modes, ν_{19}, ν_{20}, and ν_{26}, which we were able to record with Q-band excitation for both the neutral parent and the anion (Figure 7). The former shows no intensity in parallel polarization ($\rho = \infty$), but the latter shows significant parallel intensity, giving ρ values of 1.4−2. This is direct evidence for a static distortion.

The 27 cm^{-1} Upshift of ν_{19}: Direct Evidence for B_{1g} Distortion. Metalloporphyrin anion radicals can undergo B_{1g} or B_{2g} Jahn−Teller distortions when one electron is added to the e_g* LUMO's,[38] as shown in Figure 9. Differences in bond stretching force constants (bold, mdyn/Å) and bond lengths (italic, Å) between (OV)TPP and the anion radical are also superimposed on the orbital diagram for a B_{1g} distortion (Figure 9a). The bond length changes were obtained by scaling bond stretching force constants according to the Burgi−Dunitz relationship.[42] The key differences between these two distortions are the bond order changes of the $C_\alpha-C_m$ and $C_\beta-C_\beta$ bonds. In a B_{1g} distortion, one pair of $C_\beta-C_\beta$ bonds is weakened while the other pair is slightly strengthened. Likewise, the $C_\alpha-C_m$ bonds are divided into two sets, one of which is weakened while the other is strengthened. In contrast, all four $C_\beta-C_\beta$ bonds are weakened in a B_{2g} distortion which is produced by a configuration interaction product of two Eg* orbitals. Moreover, none of the $C_\alpha-C_m$ bonds are strengthened

(43) Donohoe, R. J.; Atamian, M.; Bocian, D. F. *J. Phys. Chem.* **1989**, *93*, 2244.

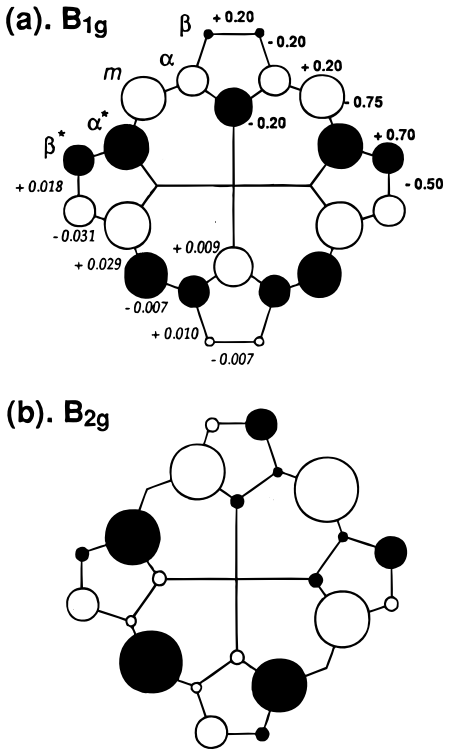

Figure 9. Orbital pattern for (a) a B_{1g} distortion (one of the e_g* orbitals) and (b) a B_{2g} distortion (linear combination of the two e_g* orbitals). Estimated changes in bond stretching force constants (bold, mdyn/Å) and bond lengths (italic, Å) upon one-electron reduction are superimposed on the B_{1g} pattern. The bond length changes were obtained by scaling the stretching force constants according to the Burgi−Dunitz relationship.[42] The sizes of the circles are proportional to the orbital coefficients.[38]

in a B_{2g} distortion; four of them are unaffected because of the nodes at the C_m positions, and four weaken slightly.

The 27 cm^{-1} upshift of the ν_{19} mode, a nearly pure $C_\alpha-C_m$ vibration, establishes that some of the $C_\alpha-C_m$ bonds are strengthened. This is direct evidence for a B_{1g} distortion because $C_\alpha-C_m$ bond orders cannot be increased by a B_{2g} distortion. In addition, the disparate frequency shifts of several $C_\beta-C_\beta$ (ν_2 and ν_{11}) and $C_\alpha-C_m$ (ν_{10} and ν_{19}) stretching modes also support a B_{1g} distortion for $(OV)TPP^-$. Among these modes, both ν_{10} and ν_{19} are nearly pure $C_\alpha-C_m$ bond stretching modes, having the same local coordinates but differing in their phasing (Figure 8); however, they shifted in opposite directions upon one-electron reduction. The normal-mode calculation for $(OV)TPP^-$ shows that ν_{19} has a greater contribution from the strengthened $C_\alpha-C_m$ bonds, which produces the 27 cm^{-1} upshift, while the downshifted ν_{10} mode is localized on the weakened $C_\alpha-C_m$ bonds (Table 3). This localization phenomenon explains the opposite frequency shifts.

Comparison with (OV)OEP. As reported previously,[24] the vanadyloctaethylporphine anion radical ($(OV)OEP^-$) also undergoes a B_{1g} Jahn−Teller distortion. As shown by normal-mode calculations, both (OV)TPP and (OV)OEP have similar degrees of structural change upon one-electron reduction. In addition, disparate frequency shifts of vibrational modes can be found in both cases. However, there is a noticeable difference: the bond stretching force constant of the strengthened $C_\alpha-C_\beta$ bonds increases more in the case of the (OV)TPP anion radical than in the case of the (OV)OEP anion radical. This larger $C_\alpha-C_\beta$ bond order increase results in an upshift of the ν_4 mode upon reduction of (OV)TPP, whereas the mode shifts down in (OV)OEP. A similar upshift of the ν_4 mode has also been reported for the MgTPP anion radical.[15]

O−V Stretching. Another interesting feature in the RR spectra of (OV)TPP is the presence of the O−V stretching mode.[44] For the neutral species, this mode is found at 992 cm^{-1}, which indicates that (OV)TPP is 5-coordinated in the THF solution.[39,40] Upon one-electron reduction, this mode shifts down by 12 cm^{-1}. This is the expected direction because the addition of one electron to the porphyrin LUMO increases the electron density at the pyrrole nitrogen atoms. Consequently, the porphyrin ring becomes a stronger electron-donating ligand and competes more effectively with the O→V donor interaction, weakening the V═O bond.

Acknowledgment. This work was supported by National Institutes of Health Grant 33576.

IC960381A

(44) This mode was not observed in (OV)OEP,[24] probably because of overlay with a solvent band.